NASA
Technical
Paper
2659

February 1987

Doubly Differential Cross Sections for Galactic Heavy-Ion Fragmentation

Francis A. Cucinotta,
John W. Norbury,
Govind S. Khandelwal, and
Lawrence W. Townsend

NASA

NASA Technical Paper 2659

1987

Doubly Differential Cross Sections for Galactic Heavy-Ion Fragmentation

Francis A. Cucinotta,
John W. Norbury, and
Govind S. Khandelwal
Old Dominion University
Norfolk, Virginia

Lawrence W. Townsend
Langley Research Center
Hampton, Virginia

National Aeronautics
and Space Administration

Scientific and Technical Information Branch

Introduction

For career astronauts and long-duration missions, the high-energy heavy-ion component of galactic cosmic rays may cause harmful radiobiological effects. To assess these effects, an accurate theoretical description of the transport of high-energy nuclei through spacecraft structures is being developed (ref. 1). An essential part of this transport theory is the description of the fragmentation that occurs in a high-energy, or relativistic, heavy-ion collision. Relativistic heavy-ion (RHI) collisions are divided into peripheral, in which there is small overlap between colliding projectile and target nuclei, and central, in which there is near or complete overlap between projectile and target. The peripheral collisions are distinguished (ref. 2) by projectile fragments observed in the forward direction that are close in mass number and velocity to that of the projectiles and by smaller fragments observed at large angles. In the much more violent central collisions, a multiplicity of small fragments are distributed isotropically. The combination of a much higher probability (ref. 3) for a peripheral event (approximately 90 percent) and the larger, higher energy peripheral fragments makes the description of peripheral collisions most important for space radiation protection.

A previous paper (ref. 4) presented an abrasion-ablation T-matrix formulation for the description of projectile fragmentation in peripheral RHI collisions. The abrasion-ablation model used is illustrated by the schematic diagram of figure 1. Here the abrasion stage is represented by the interaction of the projectile P and target T, exciting these into the projectile and target prefragment states, P' and T'. To simplify the calculations, the removed or abraded nucleons from P and T in the abrasion stage are represented by one fireball piece R. As a further simplification, only the ablation stage for the projectile prefragment is considered as shown by the decay of P' into the final projectile fragment Z and ablated piece X. (An equivalent treatment of target fragmentation follows simply by interchanging roles of projectile and target.) The diagram of figure 1 shows abrasion-ablation interactions to only first order. The T-matrix formalism allows for consideration of interactions to infinite order and incorporates ablation effects in a more fundamental way than previous treatments (refs. 5–7). Individual abrasion and ablation T-matrices were shown to factor out in reference 4, so that an optical model could be used to describe the abrasion stage (refs. 8–10). The main obstacle left in the application of this formalism is the calculation of the ablation T-matrix.

In this work we use a parameterization of the ablation T-matrix to fit doubly differential cross sections for projectile fragmentation in collisions of ^{12}C onto ^{12}C and ^{108}Ag at 86 MeV/nucleon, and ^{16}O onto ^{9}Be at 2.1 GeV/nucleon. Two parameters used in our calculations are the overall heights of the cross-sectional curves and a total width associated with the prefragment, or intermediate, state. Fits of this width allow us to make predictions of the lifetime of the intermediate state. A width associated with an exponential parameterization of the ablation T-matrix is treated both as a parameter and as a temperature which is calculated as a function of the excitation energy of the prefragment. The fits of this work are compared with previous ones. In the next section, we review the abrasion-ablation T-matrix formalism; then we describe the method of evaluating Lorentz invariant and doubly differential cross sections; and finally we discuss our comparisons with experimental results and previous treatments.

Abrasion-Ablation T-Matrix

From reference 4 the full interaction potential V for the fragmentation process is separated into individual abrasion and ablation pieces V^1 and V^2, respectively. The T-matrix expansion for abrasion-ablation (AA) is

$$\begin{aligned} T_{ki}^{AA} &= V_{ki}^1 + V_{kn}^1 G_{ni} V_{ni}^1 \\ &\quad + V_{kn}^2 G_{ni} V_{ni}^1 \\ &\quad + V_{kn}^1 G_{ni} V_{ni}^2 + V_{kn}^2 G_{ni} V_{ni}^2 + \ldots \end{aligned} \tag{1}$$

where G is the Green's function; subscript i indicates the initial state, k the final state, and n the intermediate state; and an Einstein summation convention on triply repeated indices is implied. In reference 4, diagram techniques, including a time-ordering approximation to assure causality between abrasion and ablation, were used to show that the abrasion-ablation T-matrix reduces to

$$T_{ki}^{AA} = T_{kn}^{\mathrm{abl}} G_{ni} T_{ni}^{\mathrm{abr}} \tag{2}$$

where T_{kn}^{abl} and T_{ni}^{abr} are the T-matrix expansions for ablation and abrasion, respectively. This is an extremely useful result as it allows the infinite-order ablation process as represented by T_{kn}^{abl} to be incorporated into a previously developed infinite-order abrasion formalism.

The T-matrix is simply related to the transition rate and total cross section for the fragmentation process. The Lorentz invariant differential cross section, as derived in reference 4, is most useful because once calculated, doubly differential, singly

differential, and the total cross sections can be easily evaluated using algebraic relations and numerical integration. The Lorentz invariant differential cross section for the production of a projectile fragment Z is

$$\frac{d^3\sigma(Z)}{c^3(dp^3/\varepsilon)_Z} = \frac{\varepsilon_Z}{c^3}\,\frac{2\pi\nu}{\hbar v}\,\frac{\nu^3}{(2\pi\hbar)^9} \times \frac{d}{d_{\varepsilon_{ZXRT'}}}\int\int |T^{\rm abl}_{kn}\; G_{ni}\; T^{\rm abr}_{ni}|^2 d^3p_{P'} d^3p_{T'} \quad (3)$$

where $\hbar$ is Planck's constant, ν is a normalization volume, and v the incident projectile velocity. For convenience we use the notation

$$d\sigma_{\rm inv}(Z) = \frac{d^3\sigma(Z)}{c^3(dp^3/\varepsilon)_Z} \quad (4)$$

Using the classical probability approximation which ignores all interference terms (discussed in ref. 4),

$$|T^{\rm abl}_{kn} G_{ni} T^{\rm abr}_{ni}|^2 \approx |T^{\rm abl}_{kn}|^2 |G_{ni}|^2 |T^{\rm abr}_{ni}|^2 \quad (5)$$

and expressing the abrasion T-matrix in terms of the total abrasion cross section $\sigma_n(A)$, equation (3) becomes

$$d\sigma_{\rm inv}(Z) = \frac{\varepsilon_Z}{c^3}\,\frac{\nu}{(2\pi\hbar)^3} |T^{\rm abl}_{kn}|^2 |G_{ni}|^2 \sigma_n(A) \quad (6)$$

Then inserting the Green's function through

$$|G_{ni}|^2 = \frac{1}{(\varepsilon_n - \varepsilon_i)^2 + (\Gamma/2)^2} \quad (7)$$

where Γ is the total width for all intermediate states (projectile prefragments), we have

$$d\sigma_{\rm inv}(Z) = \frac{\varepsilon_Z}{c^3}\,\frac{\nu}{(2\pi\hbar)^3}\,\frac{|T^{\rm abl}_{kn}|^2 \sigma_n(A)}{(\varepsilon_n - \varepsilon_i)^2 + (\Gamma/2)^2} \quad (8)$$

Equation (8) is the basis from which all numerical calculations are made in this report. Doubly differential cross sections are calculated from

$$\left[\frac{d^2\sigma(Z)}{d\,p\,d\Omega}\right]_{\rm frame} = \left(\frac{p^2c^3}{\varepsilon}\right)_{\rm frame} d\sigma_{\rm inv}(Z) \quad (9)$$

and

$$\left[\frac{d^2\sigma(Z)}{d\varepsilon\,d\Omega}\right]_{\rm frame} = (pc)_{\rm frame} d\sigma_{\rm inv}(Z) \quad (10)$$

The subscript frame in equations (9) and (10) denotes that the specific quantity is evaluated in the desired reference frame, which is completely arbitrary.

Method of Evaluation

The calculation of Lorentz invariant differential cross sections for the production of a projectile fragment Z as given by equation (8) involves three main factors: the abrasion cross section $\sigma_n(A)$, the ablation T-matrix $T^{\rm abl}_{kn}$, and the Green's function G_{ni}. Calculation of each of these factors is described in this section. We evaluate $d\sigma_{\rm inv}(Z)$ in the rest frame of the projectile as a function of the fragment's 4-momentum. The experimental results for the doubly differential cross sections that are used for comparison are given in the lab frame. It is important to note (ref. 11) that the procedure for evaluation of $d\sigma_{\rm inv}(Z)$ is to specify the fragment's 4-momentum in the lab frame and to Lorentz transform this to the projectile frame where $d\sigma_{\rm inv}(Z)$ is then evaluated.

The projectile frame (fig. 2) is defined to be moving parallel to the lab frame with a velocity $\beta = v/c$, which is determined by the incident kinetic energy K of the projectile per nucleon through (ref. 12)

$$\gamma = \frac{1}{(1-\beta^2)^{1/2}} \quad (11)$$

and

$$\gamma = 1 + \frac{K}{m_N} \quad (12)$$

where m_N is the nucleon mass ($m_N = 939$ MeV/c^2), and the speed of light c is set equal to 1. With projectile frame quantities represented by barred symbols and lab frame quantities by symbols without bars, the needed transformation equations are

$$\bar{p} = \left[p^2 \sin^2\theta + \gamma^2 (p\cos\theta - \beta\varepsilon)^2\right]^{1/2} \quad (13)$$

$$\bar{\varepsilon} = \left[p^2 + m^2\right]^{1/2} \quad (14)$$

$$\tan\bar{\theta} = \frac{p\sin\theta}{\gamma(p\cos\theta - \beta\varepsilon)} \quad (15)$$

Abrasion Cross Sections

Details of the calculation of abrasion cross sections using an optical model potential approximation to the exact nucleus-nucleus multiple scattering series can be found in references 8 to 10; here we

summarize the main results. The cross section for abrading n projectile nucleons is

$$\sigma_n = \binom{A_P}{n} \int d^2\mathbf{b}\,[1 - P(\mathbf{b})]^n \; P(\mathbf{b})^{A_{P'}} \qquad (16)$$

where $\mathbf{b}$ is the impact parameter vector, A_P and $A_{P'}$ are the projectile and projectile prefragment mass numbers, respectively, and $P(\mathbf{b})$ is the probability of not removing a projectile nucleon in the collision,

$$P(\mathbf{b}) = \exp\left[-A_P \sigma(e)\; I(\mathbf{b})\right] \qquad (17)$$

with

$$I(\mathbf{b}) = [2\pi B(e)]^{-3/2} \int dz^3 \int d^3\xi_T \rho_T(\boldsymbol{\xi}_P) \int d^3y\, \rho_P(\mathbf{b} + \mathbf{z} + \mathbf{y} + \boldsymbol{\xi}_T) \times \exp\left[\frac{-y^2}{2B(e)}\right] [1 - C(\mathbf{y})] \qquad (18)$$

where $\mathbf{z}$ is the position vector of the projectile, $\boldsymbol{\xi}$ is the collection of relative coordinates, and $\mathbf{y}$ is the two-nucleon relative position vector. Methods for determining the appropriate nuclear distributions ρ_T and ρ_P and constituent-averaged nucleon-nucleon cross sections $\sigma(e)$ are described in references 13 and 14. Values for the nucleon-nucleon scattering slope parameter $B(e)$ are obtained from the parameterization, appropriate for diffractive scattering, given in reference 15. The Pauli correlation is

$$C(\mathbf{y}) = 0.25 \exp\left(-K_F^2 y^2/10\right) \qquad (19)$$

where the Fermi momentum is

$$K_F = 1.36 \text{ fm}^{-1}$$

Results are obtained using numerical integration techniques.

Since the abraded nucleons consist of protons and neutrons, a prescription for calculating the charge dispersions of the prefragments is needed in order to calculate final isotope cross sections. Two such prescriptions exist: a hypergeometric distribution and a model based on the zero-point vibrations of the giant dipole resonance of the projectile nucleus. These are described in reference 16. For the calculations of this paper we use the hypergeometric distribution. Results are listed in table 1.

Ablation T-Matrix

The ablation T-matrix T_{kn}^{abl} describes the decay of the projectile prefragment into the final projectile fragment. Difficulties arise in the calculation of T_{kn}^{abl} due to lack of knowledge of intermediate state wave functions and of the ablation interaction. Information on the type of decay, such as pre-equilibrium or equilibrium, and accurate values for the excitation energy of the prefragment would be of great assistance in formulating a model for this calculation. For this work we looked for a simple functional parameterization of T_{kn}^{abl} which would agree well with experimental results so that some information on the ablation process could be learned. Various exponentials and moments of exponentials in the fragment's energy and momentum were studied, with consistently good agreement, discussed below, found only for the form,

$$|T_{kn}^{\text{abl}}|^2 \propto e^{-\overline{K}_Z/\varepsilon_0} \qquad (20)$$

which through

$$\overline{K}_Z = \frac{\bar{p}_Z^2}{2m_Z} \qquad (21)$$

is equivalent to

$$|T_{kn}^{\text{abl}}|^2 \propto e^{-\bar{p}_Z^2/2\Delta^2} \qquad (22)$$

where $\overline{K}_Z$ and $\bar{p}_Z$ are projectile frame kinetic energy and momentum, respectively. The slope parameter ε_0 and Gaussian width Δ are related by

$$\Delta = \sqrt{m_Z \varepsilon_0} \qquad (23)$$

The forms used for T_{kn}^{abl} are difficult to interpret precisely. Gaussian shapes have been used in the description of projectile fragmentation in the framework of shell model, harmonic oscillator, wave functions in both a sudden approximation (ref. 17), and a Glauber theory abrasion-ablation model (ref. 7). A Gaussian width has also been related to the internal momentum distribution of the projectile nucleus (ref. 18). The form given in equation (20) could also be interpreted as arising from an equilibrium decay of the prefragment. The slope parameter would then be the temperature of the prefragment. Because the physical interpretation of the form assumed in equation (20) or (22) is not clear, we treat ε_0 both as a parameter and as a temperature. The temperature can be related to the excitation energy ε^* (ref. 19) of P' through

$$\varepsilon^* = aT_n^2 \qquad (24)$$

where a is a level density constant given by (ref. 20)

$$a = \frac{A_Z}{8 \text{ MeV}} \qquad (25)$$

The excitation energy of the prefragment is assumed to be the result of two contributions: a surface

energy term $\varepsilon_{\text{surf}}$ due to the excess surface area of P' and an energy term from frictional spectator interactions (FSI) ε_{FSI} which consists of abraded nucleons passing through P' and depositing energy. Thus

$$\varepsilon^* = \varepsilon_{\text{surf}} + \varepsilon_{\text{FSI}} \tag{26}$$

Details of the calculation of these energies are given in reference 21. Note that ε^* must be considered an average energy as it depends on both the impact parameter of the nucleus-nucleus collision and the probability and trajectory of the FSI.

Evaluation of Green's Function

The Green's function G_{ni} as given in equation (7) is a Lorentzian form with a full width at half maximum Γ. From reference 4, Γ may be calculated as a summation over partial widths Γ_{nk} corresponding to transitions from all intermediate states n to a particular final state k if the ablation T-matrix is known. For this paper we treat Γ as a parameter. Fits of Γ to experimental data allow us to predict the lifetime of the intermediate state through the uncertainty principle.

In reference 4 the energy term in equation (7) was shown to be equivalent to

$$\varepsilon_n - \varepsilon_i = \varepsilon_{P'} - \varepsilon_Z - \varepsilon_X \tag{27}$$

which indicates a variable, intermediate, virtual resonance energy $\varepsilon_{P'}$ centered about $\varepsilon_X + \varepsilon_Z$. Equation (27) must be expressed as a function of the 4-momentum of Z in the projectile frame. In terms of kinetic energy, rest mass energy, and the prefragment excitation energy,

$$\begin{aligned}\varepsilon_n - \varepsilon_i = {} & K_{P'} + \varepsilon^* + m_{P'} \\ & - K_Z - m_Z - K_X - m_X\end{aligned} \tag{28}$$

and defining

$$Q = m_{P'} - m_Z - m_X \tag{29}$$

we have

$$\varepsilon_n - \varepsilon_i = K_{P'} + \varepsilon^* - K_Z - K_X + Q \tag{30}$$

With conservation of mass number assumed,

$$A_{P'} = A_Z + A_X \tag{31}$$

and with B representing binding energy,

$$Q = B_Z + B_X - B_{P'} \tag{32}$$

For the inclusive experimental results under study, the exact nature of X is not known and cannot be specified. For example, if $A_X = 2$, X may consist of two free nucleons or a nucleus with mass number 2; consequently, B_X is not known. Since we consider light projectiles, ^{12}C and ^{16}O, where only a small number of nucleons are emitted in the ablation stage, we take

$$B_X = 0 \tag{33}$$

For $B_{P'}$ and B_Z we use the approximation (ref. 19)

$$\frac{B}{A} = 8 \text{ MeV} \tag{34}$$

Then Q becomes

$$Q = -8A_X \tag{35}$$

To obtain expressions for $K_{P'}$ and K_X in terms of K_Z, we treat the ablation process, in the prefragment frame (fig. 3), as an isotropic, two-body decay of P' into Z and X. In this frame, K_Z and K_X can be found in terms of rest mass energies and the excitation energy. Knowledge of K_Z in the projectile frame, where it is specified, and in the prefragment frame gives us the velocity of the prefragment P' relative to the projectile P. The particle X is considered to move with the center-of-mass velocity of all ablated particles with a mass $A_X m_N$. Nonrelativistic kinematics is used because the relative velocity between projectile and prefragment frames is much less than the speed of light. (A relativistic kinematical treatment is given in the appendix.)

With barred symbols representing projectile frame values and primed symbols prefragment frame values, we have by conservation of energy in the prefragment frame

$$\varepsilon'_{P'} = \varepsilon'_Z + \varepsilon'_X \tag{36}$$

which expands to

$$K'_{P'} + m_{P'} + \varepsilon^* = K'_Z + m_Z + K'_X + m_X$$

Using the approximation for mass terms discussed above (eq. (35)) and defining U by

$$U = \varepsilon^* - 8A_X \tag{37}$$

we have

$$U = K'_Z + K'_X \tag{38}$$

or equivalently

$$U = \frac{1}{2} m_Z {v'_Z}^2 + \frac{1}{2} m_X {v'_X}^2 \tag{39}$$

Applying conservation of 3-momentum in the prefragment frame

$$\mathbf{0} = \mathbf{p}'_Z + \mathbf{p}'_X \tag{40}$$

which implies that

$$m_X v'_X = -m_Z v'_Z \tag{41}$$

Then from equation (39)

$$v'_Z = \sqrt{\frac{2U}{m_Z\left(1+\frac{m_Z}{m_X}\right)}} \tag{42}$$

The velocity of the prefragment as seen in the projectile frame is equivalent to the relative velocity between projectile and prefragment frames. Using the Galilean transformation equations, we have

$$\mathbf{v}'_Z = \bar{\mathbf{v}}_Z + \mathbf{v}_{\mathrm{rel}} \tag{43}$$

or

$$v'^{\,2}_Z = \bar{v}^2_Z + v^2_{\mathbf{rel}} + 2\bar{v}_Z v_{\mathbf{rel}} \cos\phi \tag{44}$$

where ϕ is the angle between the velocity vectors $\bar{\mathbf{v}}_Z$ and $\mathbf{v}_{\mathrm{rel}}$. Similarly,

$$\mathbf{v}_X = \bar{\mathbf{v}}_X + \mathbf{v}_{\mathrm{rel}} \tag{45}$$

or

$$v'^{\,2}_X = \bar{v}^2_X + v^2_{\mathrm{rel}} + 2\bar{v}_X v_{\mathrm{rel}} \cos\alpha \tag{46}$$

where α is the angle between the velocity vectors $\mathbf{v}_X$ and $\mathbf{v}_{\mathrm{rel}}$. There is insufficient information within our model to determine the angles ϕ and α except for the special case when the fragment Z is detected at a scattering angle θ of 0°. Here we may assume that P' and Z are moving parallel to each other in both lab and projectile frames, so that $\phi = 0°$ and $\alpha = 180°$. For the experimental results for ^{16}O on ^{9}Be at 2.1 GeV/nucleon, all fragments were detected at $\theta_{\mathrm{lab}} = 0°$. The experimental results for ^{12}C on ^{12}C and ^{12}C on $^{\mathrm{nat}}$Ag are for fragments detected at $\theta_{\mathrm{lab}} = 4°$ and $\theta_{\mathrm{lab}} = 3°$, respectively. In all cases we assume that $\phi = 0°$ and $\alpha = 180°$. With this approximation we find that

$$v_{\mathrm{rel}} = \bar{v}_{P'} = v'_Z - \bar{v}_Z \tag{47}$$

and thus

$$\overline{K}_{P'} = \frac{1}{2} m_{P'} \left[\bar{v}_Z - \sqrt{\frac{2U}{m_Z\left(\frac{1+m_Z}{m_X}\right)}}\right]^2 \tag{48}$$

Similarly,

$$\bar{v}_X = v_{\mathrm{rel}} + v'_X \tag{49}$$

which leads to

$$\overline{K}_X = \frac{1}{2} m_X \left\{\left(1-\frac{m_Z}{m_X}\right)\left[\frac{2U}{m_Z\left(\frac{1+m_Z}{m_X}\right)}\right]^{1/2} - \bar{v}_Z\right\}^2 \tag{50}$$

The expressions for $Q, \overline{K}_{P'}$, and $\overline{K}_X$ given by equations (35), (48), and (50) are used to evaluate the Green's function as a function of the fragment variables. The kinematical model used involves many approximations such as assumptions on scattering angles of the various reaction products, neglect of Coulomb effects, and the assumption of simultaneous emission of all ablated particles. The assumption of one value for the excitation of P' is also an approximation as in actuality a particular prefragment may have various values for its excitation energy. The distribution of values for ε^* is expected to have a maximum of about 100 MeV for the prefragments studied, and thus any error in choosing ε^* introduces only a small error in equations (48) and (50). These approximations are necessary in order to compare with experimental results, but eventually a quantum mechanical calculation of the energy terms must be made.

Results and Discussion

As a first application of the abrasion-ablation T-matrix formalism, we have made two- and three-parameter fits to experimental results of $d^2\sigma/dp\,d\Omega$ for projectile fragments in ^{16}O on ^{9}Be collisions at 2.1 GeV/nucleon (ref. 22) and of $d^2\sigma/d\varepsilon\,d\Omega$ for projectile fragments in ^{12}C on ^{12}C (ref. 23) and ^{12}C on $^{\mathrm{nat}}$Ag (ref. 24) collisions at 86 MeV/nucleon. For the ^{12}C on $^{\mathrm{nat}}$Ag reaction, we assume a target of ^{108}Ag. The normalization of the experimental curves is reported only for ^{12}C on ^{12}C with arbitrary units used in the other results. All the experimental curves have simple bell shapes and were fit to good agreement by our two-parameter model as shown in figures 4 to 6. A nearly identical fit is made with the three-parameter model discussed below. The excitation energies and corresponding temperatures used are listed in table 2. In our kinematical model, there was insufficient excitation energy for a prefragment state with $A = 15$ for ^{10}C and with $A = 11$ for ^{7}Be. Table 3 lists the fitted values of the total width Γ for each projectile fragment versus T_n of the two-parameter model, and table 4 lists fitted values of Γ versus ε_0 the slope parameter of our three-parameter model. The values of ε_0 and the corresponding values

of Γ listed all produce a fit nearly identical to our two-parameter fit shown in figures 4 to 6. We were unable to obtain a three-parameter fit at $\varepsilon_0 = 2$ for ^{11}C in the ^{16}O on ^{9}Be reaction and for ^{10}B and ^{7}Be in the ^{12}C on ^{12}C reaction.

The fits were made to reproduce the experimental curves in their central regions. Reasonable agreement is found in the high- and low-momentum tails for the C fragments of ^{16}O, the low-momentum tail of ^{12}C (fig. 4(c)), and high-momentum tail of ^{10}C (fig. 4(e)) being exceptions. Some deviation is seen in general for the high- and low-energy tails of the lower energy reactions (figs. 5 and 6). The peaks of all curves occur at a velocity slightly less than the projectile velocity. This phenomenon has been explained previously as the result of frictional (ref. 25) and binding energy (ref. 26) effects.

The fitted values for the total width Γ are the same order of magnitude for all fragments studied and through the uncertainty principle indicate an intermediate state lifetime τ on the order of 10^{-19} to 10^{-20} s. The widths for ^{10}B and ^{7}Be fragments from ^{12}C targets and from ^{nat}Ag targets differ by a factor of about 4, with a larger width and hence shorter lifetime for the smaller target ^{12}C. This comparison is made at slightly different scattering angles, 4° for ^{12}C and 3° for ^{nat}Ag, so that it is difficult to conclude that any target dependence has been found. The similarity in values of Γ at the two energies studied can be attributed to the comparable size of the projectiles and the similarity in excitation energies of all prefragments.

In considering the values for τ predicted from our fits to Γ, we consider two other characteristic times: $\tau_1 \approx 10^{-23}$ s (the interaction time for the abrasion stage) and $\tau_2 \approx 10^{-21}$ s (the typical period for nucleon motion in the nucleus). A rough indication of an equilibrium decay or compound nucleus decay of an excited nucleus is that the decay time be much longer than τ_2. Our predicted values for τ satisfy this criterion and thus give some justification to the use of evaporation codes for the treatment of the ablation stage, although the mode of formation of a compound nucleus state is very different from the violent nucleon knockout of abrasion. The values of τ also indicate that $\tau \gg \tau_1$ which is consistent with the use of the time-ordering approximation (ref. 4) in the formulation of the abrasion-ablation T-matrix.

From table 4, we see that as ε_0 is increased, Γ decreases, indicating a longer intermediate state lifetime for larger ε_0. This seems to contradict the interpretation of ε_0 as a temperature for which we would expect a shorter lifetime for higher temperature. As ε_0 is increased past 10 MeV, the fitted values for Γ converge to constant values. Here the exponential parameterization of T_{kn}^{abl} becomes very flat and the Green's function and kinematical factors dominate the cross-sectional distributions. In the central regions of the distributions, agreement is good for these higher values of ε_0, but agreement in the tail regions decreases.

The experimental data with which we compared our model have been parameterized previously using a simple Gaussian form (refs. 22 to 24)

$$e^{-p^2/2\Delta^2}$$

with the width Δ being the focus of much investigation (refs. 7, 17, 27 to 31). Values for Δ have been derived in one-step models of quick fragmentation (refs. 17 and 18) and of excitation followed by statistical decay (refs. 18 and 27). In reference 7, values for Δ were predicted in an abrasion-ablation model with ablation representing a correction to values for Δ derived from the abrasion step.

In figure 7 we show fits to the data for ^{11}C from the ^{16}O on ^{9}Be reaction and for ^{7}Be from the ^{12}C on ^{12}C reaction. Shown are fits from our two-parameter model, from the Gaussian form, and from the abrasion-ablation T-matrix formalism with $|T_{kn}^{abl}|^2 = 1$. All three fits reproduce the central regions and widths of the curves, with the first two being nearly identical and the fit with constant T_{kn}^{abl} deviating in the tail regions. These fits indicate that the widths of the experimental distributions do not give a strong enough indication to establish the correct model with which to describe the fragmentation process. If we denote the actual width of the distribution by w, then in the Gaussian models, w equals Δ; and in the abrasion-ablation T-matrix formalism, w is a function of T_n and Γ. The temperature T_n and Gaussian width Δ may be related through equation (23). In reference 18, the relationship between Δ and a temperature is also discussed. In the abrasion-ablation T-matrix formalism, deviation of predictions of temperature or Δ from experimental values for w in the one-step models is explained by the inclusion of the Lorentzian form that arises naturally through the Green's function that propagates between the abrasion and ablation stages.

Concluding Remarks

An exponential parameterization of the ablation T-matrix leads to good agreement with experimental results for doubly differential cross sections in fragmentation reactions involving light projectiles. Fits

to the total width for the ablation stage indicate a quick decay process, but an equilibrium decay. The importance of prefragment excitation energies is already apparent at the level of calculation of this work. Explicit calculation of the ablation T-matrix must now be conducted in order to make further progress.

NASA Langley Research Center
Hampton, Virginia 23665-5225
December 8, 1986

Appendix

Relativistic Kinematical Model

In this appendix we give the relativistic kinematical model for the calculation of energy terms in the Green's function of equation (7), which is analogous to the nonrelativistic model presented in the text. Relativistic effects increase in importance for higher values of excitation energy. For the two-body decay of P' into Z and X, assumed in the prefragment rest frame, we have the following 4-momentum

$$P_{P'} = (\varepsilon_{P'}, \mathbf{0}) \tag{A1}$$

$$P_Z = (\varepsilon_Z, \mathbf{p}_Z) \tag{A2}$$

$$P_X = (\varepsilon_X, \mathbf{p}_X) \tag{A3}$$

Through conservation we have

$$P_Z = P_{P'} - P_X \tag{A4}$$

Taking the scalar product of P_Z with itself we find

$$m_Z^2 = \varepsilon_{P'}^2 + m_X^2 - 2\varepsilon_{P'}\varepsilon_X \tag{A5}$$

Then solving for ε_X,

$$\varepsilon_X = \frac{\varepsilon_{P'}^2 + m_X^2 - m_Z^2}{2\varepsilon_{P'}} \tag{A6}$$

and inserting

$$\varepsilon_{P'} = m_{P'} + \varepsilon^* \tag{A7}$$

we have

$$\varepsilon_X = \frac{(m_{P'} + \varepsilon^*)^2 - m_X^2 - m_Z^2}{2\,(m_{P'} + \varepsilon^*)} \tag{A8}$$

Similarly we find

$$\varepsilon_Z = \frac{(m_{P'} + \varepsilon^*)^2 + m_Z^2 - m_X^2}{2\,(m_{P'} + \varepsilon^*)} \tag{A9}$$

As discussed above, we take the prefragment's velocity, as observed in the projectile frame, to be the velocity of the prefragment relative to the projectile, which is found through determination of ε_Z in both frames. By defining the lab and projectile frames as parallel, we are not free to choose the relative orientation of prefragment frame with respect to projectile frame (fig. 3). We therefore take, as the Lorentz transformation matrix between these frames, a boost in an arbitrary direction. With $A(\boldsymbol{\beta})$ the transformation matrix, we have

$$\overline{P} = A(\boldsymbol{\beta})\, P \tag{A10}$$

where $\overline{P}$ and P are projectile and prefragment frame 4-momentum, respectively. The matrix $A(\boldsymbol{\beta})$ is given by equation 11.98 of Jackson (ref. 32). Then from

$$\overline{P}_{P'} = P_{\text{rel}} = P_Z - \overline{P}_Z \tag{A11}$$

and

$$\overline{P}_X = P_X - P_{\text{rel}} \tag{A12}$$

we can formally solve for the energies $\bar{\varepsilon}_{P'}$ and $\bar{\varepsilon}_X$. Difficulties arise in that values for the parameters of the transformation matrix $A(\boldsymbol{\beta})$ cannot be determined.

References

1. Wilson, John W.: *Heavy Ion Transport in the Straight Ahead Approximation.* NASA TP-2178, 1983.
2. Nagamiya, S.; and Gyulassy, M.: High-Energy Nuclear Collisions. *Advances in Nuclear Physics, Volume 13,* J. W. Negele and Erich Vogt, eds., Plenum Press, c.1984, pp. 201–315.
3. Oliveira, Luiz F.; Donangelo, Raul; and Rasmussen, John O.: Abrasion-Ablation Calculations of Large Fragment Yields From Relativistic Heavy Ion Reactions. *Phys. Rev.*, ser. C, vol. 19, no. 3, Mar. 1979, pp. 826–833.
4. Norbury, John W.; Townsend, Lawrence W.; and Deutchman, Philip A.: *A T-Matrix Theory of Galactic Heavy-Ion Fragmentation.* NASA TP-2363, 1985.
5. Bowman, J. D.; Swiatecki, W. J.; and Tsang, C. F.: *Abrasion and Ablation of Heavy Ions.* LBL-2908, Lawrence Berkeley Lab., Univ. of California, July 1973.
6. Hüfner, J.; Schäfer, K.; and Schürmann, B.: Abrasion-Ablation in Reactions Between Relativistic Heavy Ions. *Phys. Rev.*, ser. C, vol. 12, no. 6, Dec. 1975, pp. 1888–1898.
7. Abul-Magd, A.; and Hüfner, J.: Momentum Distributions in Fragmentation Reactions With Relativistic Heavy Ions. *Z. Phys.*, ser. A, vol. 277, no. 3, 1976, pp. 379–384.
8. Wilson, J. W.: Multiple Scattering of Heavy Ions, Glauber Theory, and Optical Model. *Phys. Lett.*, vol. B52, no. 2, Sept. 1974, pp. 149–152.
9. Wilson, J. W.; and Townsend, L. W.: An Optical Model for Composite Nuclear Scattering. *Canadian J. Phys.*, vol. 59, no. 11, Nov. 1981, pp. 1569–1576.
10. Townsend, L. W.: Abrasion Cross Sections for ^{20}Ne Projectiles at 2.1 GeV/Nucleon. *Canadian J. Phys.*, vol. 61, no. 1, Jan. 1983, pp. 93-98.
11. Norbury, John William: Pion Production in Relativistic Heavy Ion Collisions. Ph.D. Diss., Univ. of Idaho Graduate School, Nov. 1983.
12. Michalowicz, A. (Scripta Technica Ltd, transl.): *Kinematics of Nuclear Reactions.* Iliffe Books Ltd (London), c.1967.
13. Townsend, Lawrence W.; Wilson, John W.; and Bidasaria, Hari B.: *Nucleon and Deuteron Scattering Cross Sections From 25 MeV/Nucleon to 22.5 GeV/Nucleon.* NASA TM-84636, 1983.
14. Townsend, Lawrence W.; Wilson, John W.; and Bidasaria, Hari B.: *Heavy-Ion Total and Absorption Cross Sections Above 25 MeV/Nucleon.* NASA TP-2138, 1983.
15. Ringia, F. E.; Dobrowolski, T.; Gustafson, H. R.; Jones, L. W.; Longo, M. J.; Parker, E. F.; and Cork, Bruce: Differential Cross Sections for Small-Angle Neutron-Proton and Neutron-Nucleus Elastic Scattering at 4.8 GeV/c. *Phys. Rev. Lett.*, vol. 28, no. 3, Jan. 17, 1972, pp. 185–188.
16. Townsend, Lawrence W.; and Norbury, John W.: *Charge-to-Mass Dispersion Methods for Abrasion-Ablation Fragmentation Models.* NASA TM-86340, 1985.
17. Lepore, Joseph V.; and Riddell, Robert J., Jr.: *Fragmentation of Heavy Nuclei at High Energy.* LBL-3086, Lawrence Berkeley Lab., Univ. of California, July 17, 1974.
18. Goldhaber, A. S.: Statistical Models of Fragmentation Processes. *Phys. Lett.*, vol. 53B, no. 4, Dec. 23, 1974, pp. 306–308.
19. Blatt, John M.; and Weisskopf, Victor F.: *Theoretical Nuclear Physics.* Springer-Verlag, c.1979.
20. Hüfner, J.: Heavy Fragments Produced in Proton-Nucleus and Nucleus-Nucleus Collisions at Relativistic Energies. *Phys. Rep.*, vol. 125, no. 4, Aug. 1985, pp. 129–185.
21. Townsend, Lawrence W.; Wilson, John W.; Cucinotta, Francis A.; and Norbury, John W.: *Optical Model Calculations of Heavy-Ion Target Fragmentation.* NASA TM-87692, 1986.
22. Heckman, Harry H.: *High-Energy Heavy Ions: A New Area for Physics Research. High-Energy Physics and Nuclear Structure,* Gunnar Tibell, ed., American Elsevier Publ. Co., Inc., 1974, pp. 403–415.
23. Mougey, J.; Ost, R.; et al.: Projectile Fragments From 86 MeV/ Nucleon ^{12}C Induced Reactions. *Phys. Lett.*, vol. 105B, no. 1, Sept. 24, 1981, pp. 25–29.
24. Mougey, Jean: Experiments With 1.03 GeV ^{12}C Ions. *Nucl. Phys.*, vol. A387, 1982, pp. 109c–127c.
25. Abul-Magd, A.; Hüfner, J.; and Schürmann, B.: Friction in Heavy Ion Reactions at Relativistic Energies. *Phys. Lett.*, vol. 60B, no. 4, Feb. 2, 1976, pp. 327–330.
26. Gugelot, P. C.: Binding Energy Correction to the Kinematics of Quasifree Scattering. *Phys. Rev.*, ser. C, vol. 30, no. 2, Aug. 1984, pp. 654–661.
27. Feshbach, H.; and Huang, K.: Fragmentation of Relativistic Heavy Ions. *Phys. Lett.*, vol. 47B, no. 4, Nov. 26, 1973, pp. 300–302.
28. Greiner, D. E.; Lindstrom, P. J.; Heckman, H. H.; Cork, Bruce; and Bieser, F. S.: Momentum Distributions of Isotopes Produced by Fragmentation of Relativistic ^{12}C and ^{16}O Projectiles. *Phys. Rev. Lett.*, vol. 35, no. 3, July 21, 1975, pp. 152–155.
29. Bertsch, G.: Pauli Suppression of Momentum Fluctuations. *Phys. Rev. Lett.*, vol. 46, no. 7, Feb. 16, 1981, pp. 472–473.
30. Friedman, William A.: Heavy Ion Projectile Fragmentation: Reexamination. *Phys. Rev.*, ser. C, vol. 27, no. 2, Feb. 1983, pp. 569–577.
31. Murphy, Martin J.: Phase-Space Constraints on the Momenta of Projectile Fragments. *Phys. Lett.*, vol. 135, no. 1, 2, 3, Feb. 2, 1984, pp. 25–28.
32. Jackson, John David: *Classical Electrodynamics,* Second ed. John Wiley & Sons, Inc., c.1975.

Symbols

a	level density constant, MeV^{-1}
A	mass number
B	binding energy, MeV
c	speed of light
$C(\mathbf{y})$	Pauli correlation
G_{ni}	Green's function matrix
$I(\mathbf{b})$	defined in equation (18)
K	kinetic energy, MeV
m	mass
$\mathbf{p}$	3-momentum
p	momentum
P	projectile (see fig. 1)
P'	projectile prefragment (see fig. 1)
R	fireball piece (see fig. 1)
T	target (see fig. 1)
T'	target prefragment (see fig. 1)
T_{kn}^{abl}	ablation T-matrix
T_{kn}^{abr}	abrasion T-matrix
T_{kn}^{AA}	abrasion-ablation T-matrix
T_n	temperature, MeV
$\mathbf{v}$	velocity vector
$\mathbf{v}_{\mathrm{rel}}$	relative velocity vector between projectile and prefragment frames
V^1	abrasion potential
V^2	ablation potential
X	ablated piece (see fig. 1)
Z	final projectile fragment (see fig. 1)
α	angle between velocity vectors $\overline{\mathbf{v}}_X$ and $\mathbf{v}_{\mathrm{rel}}$
$\boldsymbol{\beta}$	relative velocity vector between lab frame and projectile frame
Γ	total width for all intermediate states
Δ	Gaussian width
ε	energy, MeV
ε_0	slope parameter
ε^*	excitation energy, MeV
θ	scattering angle
σ	cross section
$\sigma_n(A)$	total abrasion cross section, mb
ϕ	angle between velocity vectors $\overline{\mathbf{v}}_Z$ and $\mathbf{v}_{\mathrm{rel}}$ (see eq. (44))
Ω	solid angle, sr

Subscripts:

i	initial state
k	final state
n	intermediate state

A bar over a symbol indicates the projectile frame. A prime (other than P') indicates the prefragment frame. See figures 2 and 3.

Table 1. Optical Model Abrasion Cross Sections With Hypergeometric Charge Dispersion

(a) ^{16}O + ^{9}Be at 2.1 GeV/nucleon

P'	σ_n(A), mb
^{15}O	133.5
^{15}N	133.5
^{14}O	36.1
^{14}N	82.6
^{14}C	36.1
^{13}O	10.5
^{13}N	41.8
^{13}C	41.8
^{12}O	3.2
^{12}N	20.6
^{12}C	36.1
^{11}O	.9
^{11}N	9.2
^{11}C	25.7

(b) ^{12}C + ^{12}C at 86 MeV/nucleon

P'	σ_n(A), mb
^{11}C	109.0
^{11}B	109.0
^{10}C	28.0
^{10}B	67.0
^{10}Be	28.0
^{9}C	8.0
^{9}B	36.5
^{9}Be	36.5
^{8}C	2.0
^{8}B	18.0
^{8}Be	33.0

(c) ^{12}C + ^{108}Ag at 86 MeV/nucleon

P'	σ_n(A), mb
^{11}C	157.5
^{11}B	157.5
^{10}C	40.5
^{10}B	97.3
^{10}Be	40.5
^{9}C	12.1
^{9}B	54.3
^{9}Be	54.3
^{8}C	50.5
^{8}B	26.9
^{8}Be	3.4

Table 2. Excitation Energies and Temperatures

(a) $^{16}O + {}^{9}Be$ at 2.1 GeV/nucleon

$A_{P'}$	ε^*, MeV	T_n, Mev
15	35.6	$16.8/\sqrt{A_Z}$
14	39.2	$17.7/\sqrt{A_Z}$
13	42.7	$18.5/\sqrt{A_Z}$
12	46.1	$19.2/\sqrt{A_Z}$
11	47.3	$19.4/\sqrt{A_Z}$

(b) $^{12}C + {}^{12}C$ at 86 MeV/nucleon

$A_{P'}$	ε^*, MeV	T_n, MeV
11	30	$15.5/\sqrt{A_Z}$
10	38	$17.4/\sqrt{A_Z}$
9	46	$19.2/\sqrt{A_Z}$
8	49	$19.8/\sqrt{A_Z}$

(c) $^{12}C + {}^{108}Ag$ at 86 MeV/nucleon

$A_{P'}$	ε^*, MeV	T_n, MeV
11	25.0	$14.1/\sqrt{A_Z}$
10	35.0	$16.7/\sqrt{A_Z}$
9	41.4	$18.2/\sqrt{A_Z}$
8	42.6	$18.5/\sqrt{A_Z}$

Table 3. Fitted Values for Total Width Γ Using Calculated Value of T_n in Two-Parameter Model

(a) $^{16}O + {}^{9}Be$ at 2.1 GeV/nucleon with $\theta_{lab} = 0°$

Γ, MeV for —				
^{14}C	^{13}C	^{12}C	^{11}C	^{10}C
0.018	0.014	0.03	0.048	0.027

(b) $^{12}C + {}^{12}C$ at 86 MeV/nucleon with $\theta_{lab} = 4°$

Γ, MeV for —	
^{10}B	^{7}Be
0.12	0.09

(c) $^{12}C + {}^{109}Ag$ at 86 MeV/nucleon with $\theta_{lab} = 3°$

Γ, MeV for —	
^{10}B	^{7}Be
0.03	0.02

Table 4. Fitted Values for Total Width Γ as a Function of Slope Parameter ε_0 in Three-Parameter Model

(a) $^{16}O + {}^{9}Be$ at 2.1 GeV/nucleon with $\theta_{lab} = 0°$

ε_0, MeV	Γ, MeV for —				
	^{14}C	^{13}C	^{12}C	^{11}C	^{10}C
2	0.04	0.03	0.2	(a)	0.04
3	.025	.02	.05	0.1	.03
5	.02	.015	.03	.04	.02
7	.015	.012	.025	.03	.015
10	.015	.011	.02	.03	.015

(b) $^{12}C + {}^{12}C$ at 86 MeV/nucleon with $\theta_{lab} = 4°$

ε_0, MeV	Γ, MeV for —	
	^{10}B	^{7}Be
2	(a)	(a)
3	0.5	1.0
5	.1	.15
7	.08	.08
10	.07	.06

(c) $^{12}C + {}^{108}Ag$ at 86 MeV/nucleon with $\theta_{lab} = 3°$

ε_0, MeV	Γ, MeV for —	
	^{10}B	^{7}Be
2	0.10	0.07
3	.05	.04
5	.03	.03
7	.03	.02
10	.02	.02

[a]Could not be fit with listed value of ε_0.

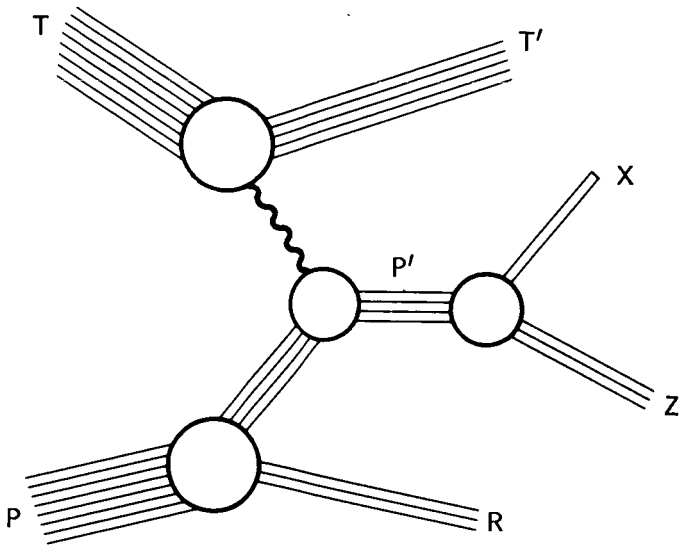

Figure 1. Diagram for projectile fragmentation in the abrasion-ablation model.

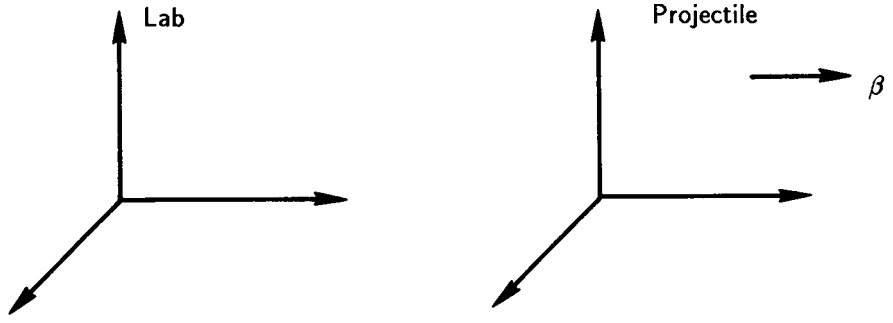

Figure 2. Relative orientation of lab and projectile frames.

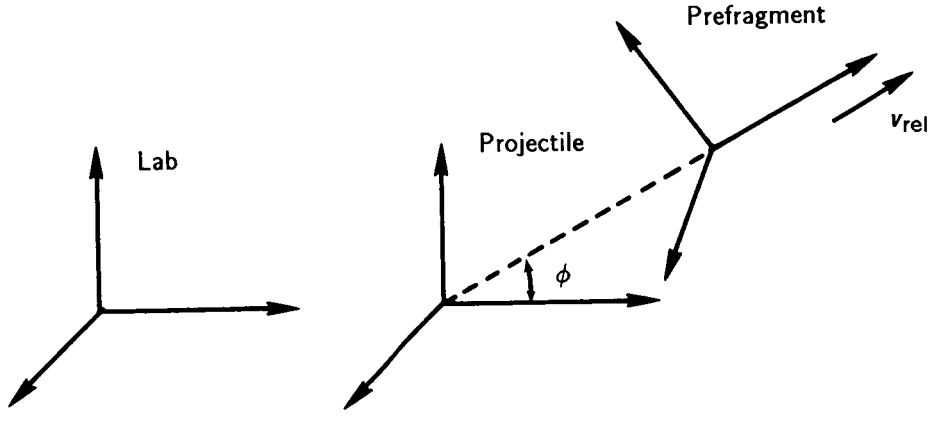

Figure 3. Orientation of prefragment frame.

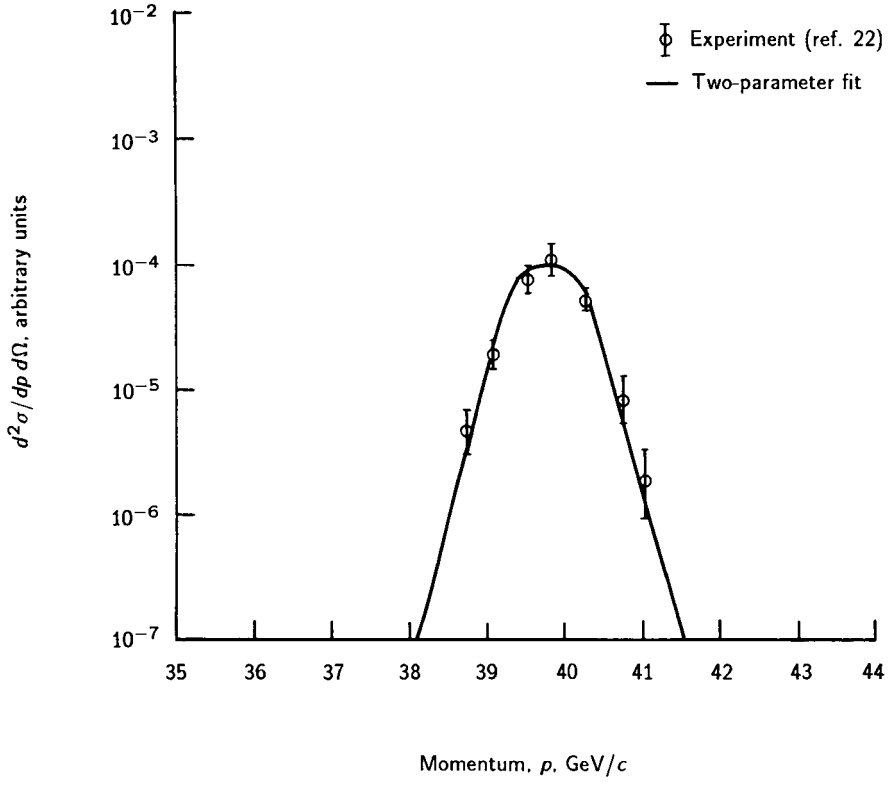

(a) For ^{14}C production.

Figure 4. Doubly differential cross section for fragment production at 0° in reaction of ^{16}O on ^{9}Be at 2.1 GeV/nucleon.

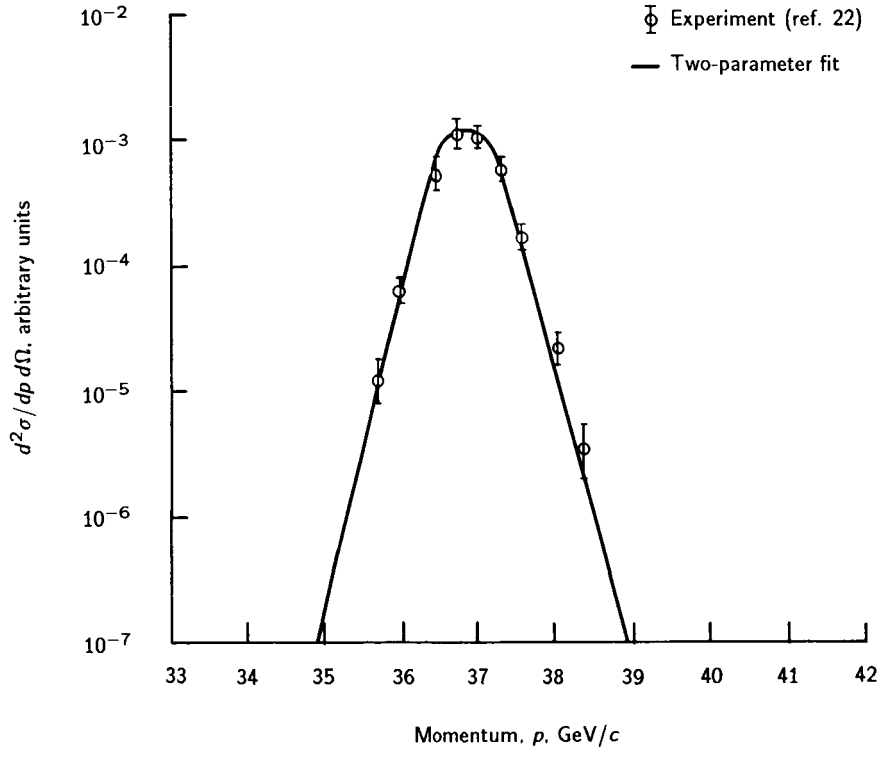

(b) For ^{13}C production.

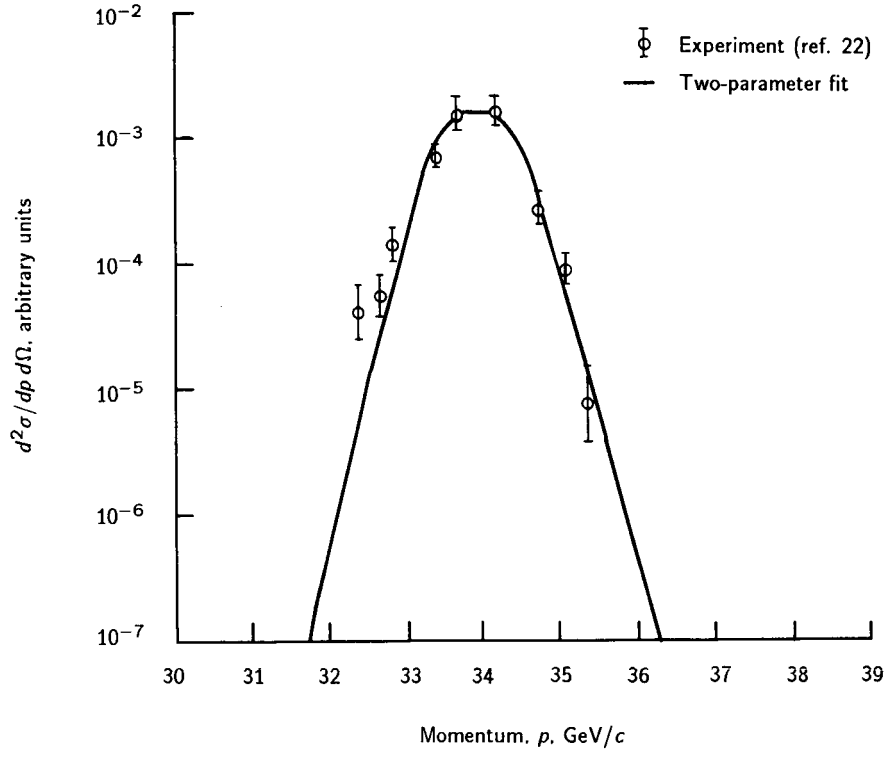

(c) For ^{12}C production.

Figure 4. Continued.

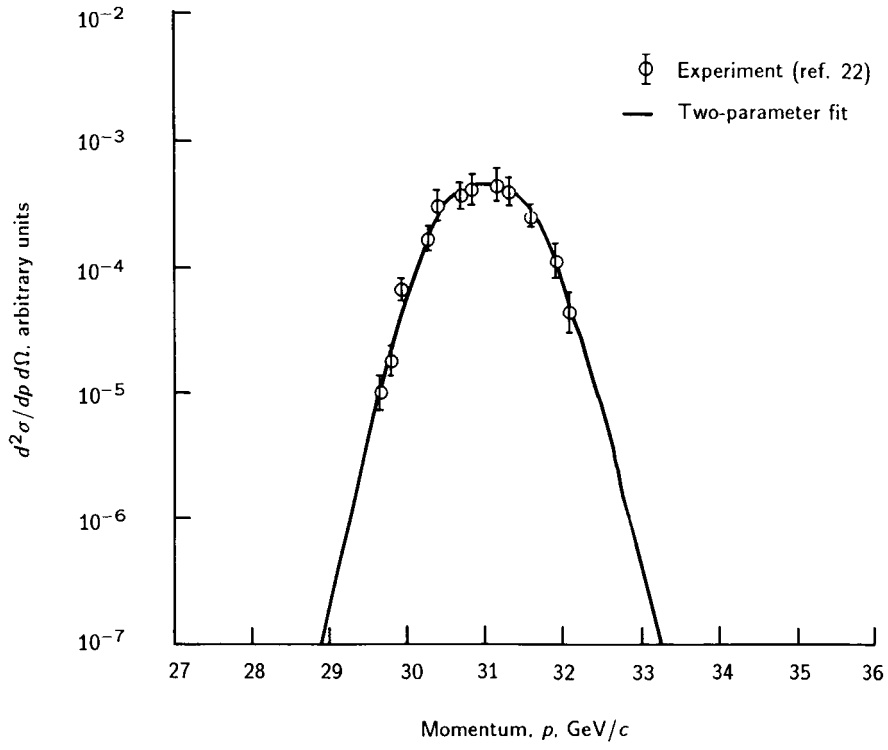

(d) For ^{11}C production.

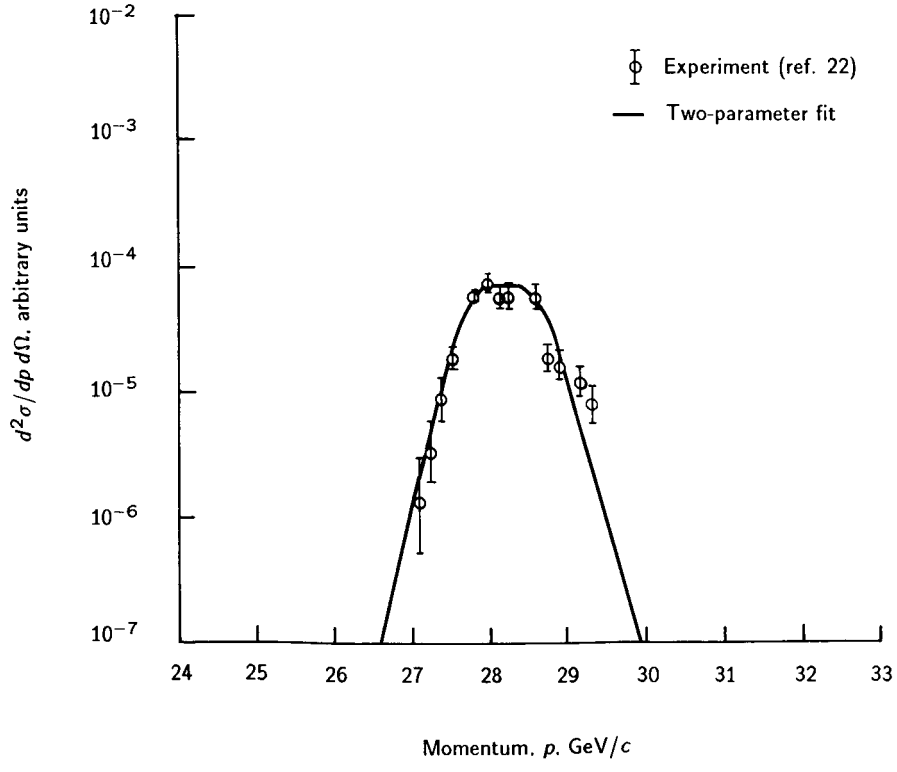

(e) For ^{10}C production.

Figure 4. Concluded.

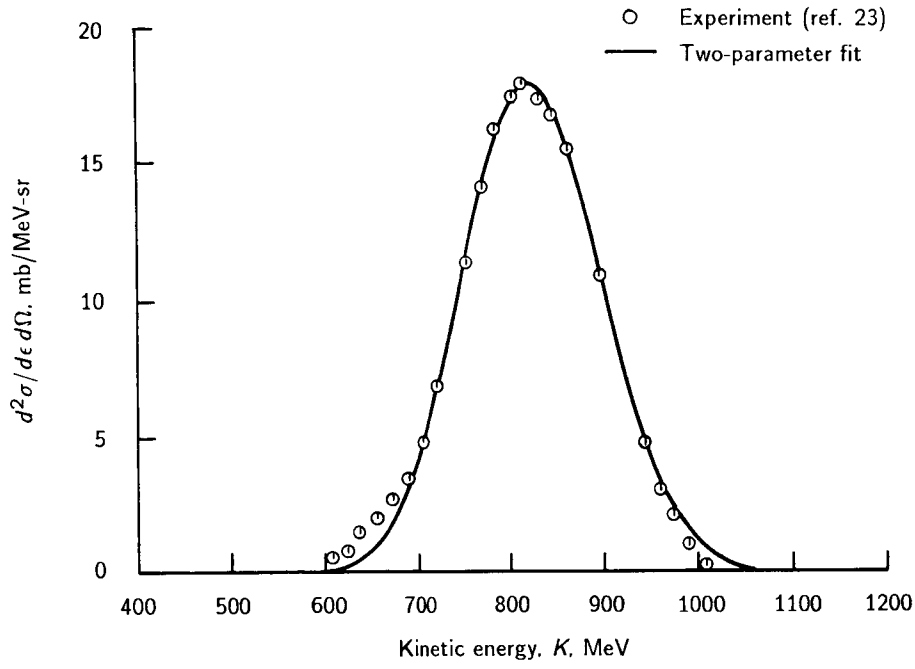

(a) For ^{10}B production.

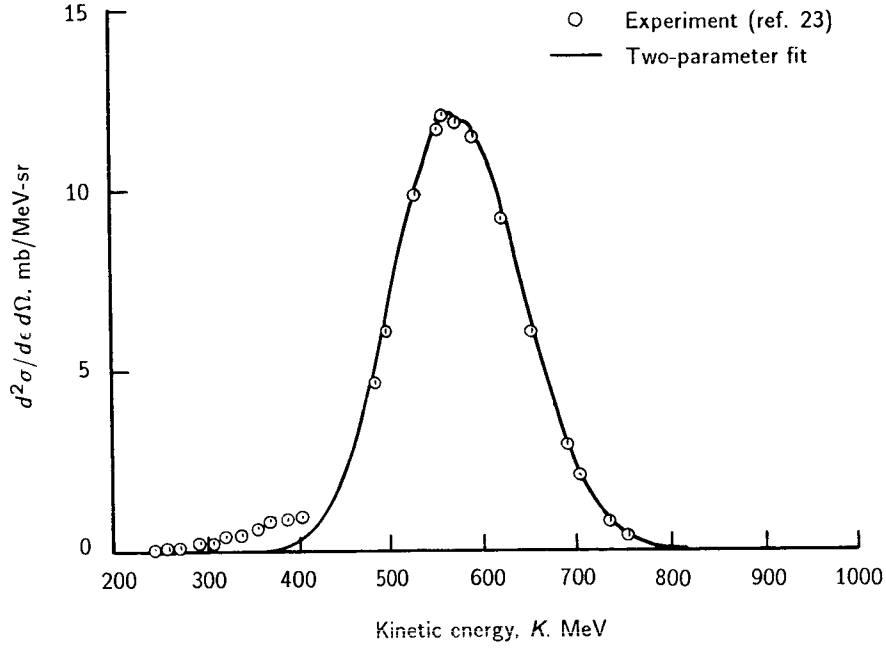

(b) For ^{7}Be production.

Figure 5. Doubly differential cross section for fragment production at 4° in reaction of ^{12}C on ^{12}C at 86 MeV/nucleon.

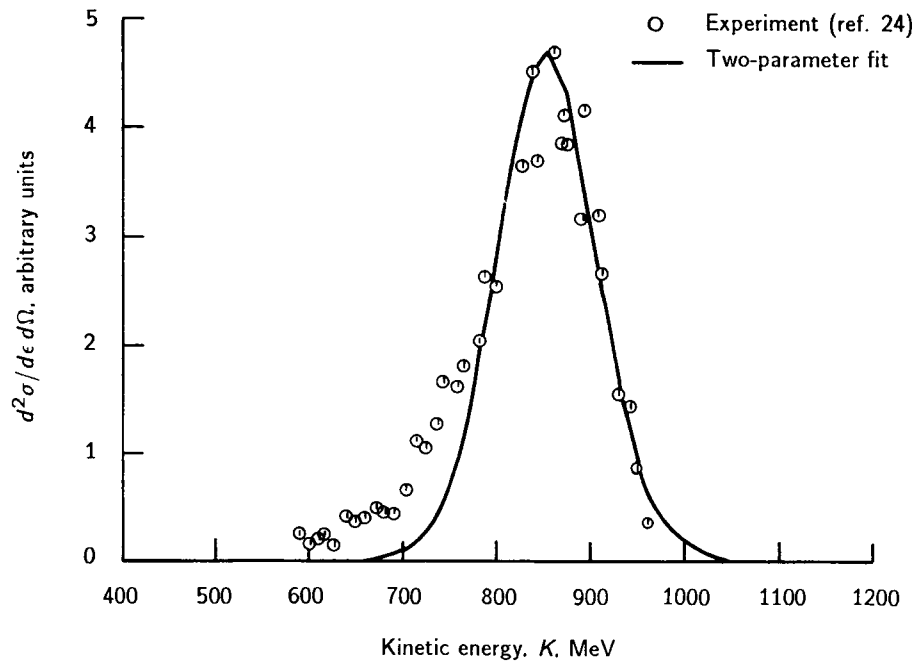

(a) For ^{10}B production.

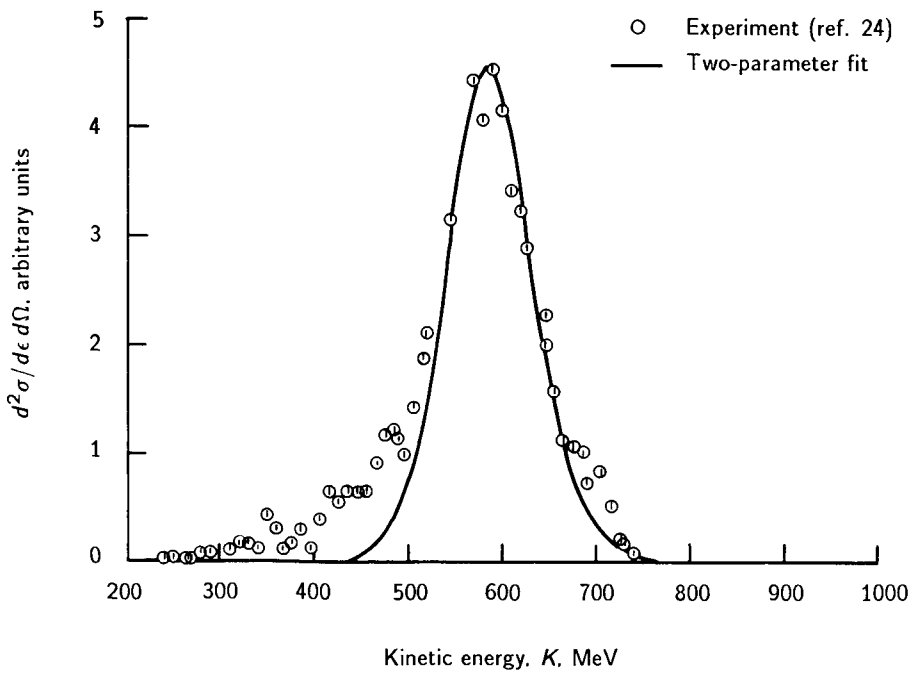

(b) For ^{7}Be production.

Figure 6. Doubly differential cross section for fragment production at 3° in reaction of ^{12}C on ^{nat}Ag at 86 MeV/nucleon.

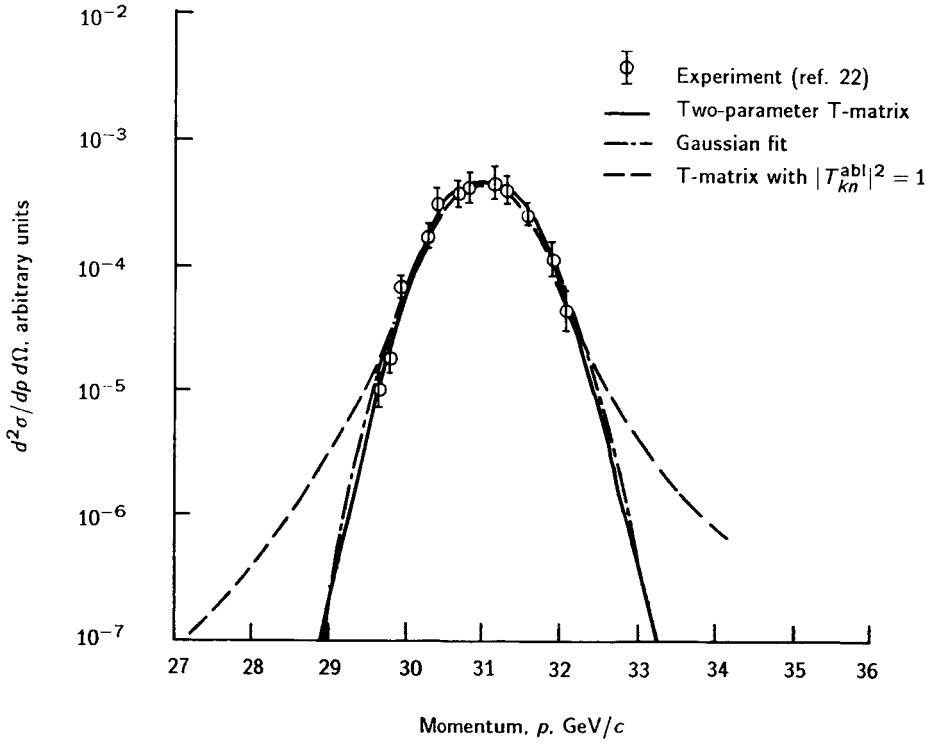

(a) For ^{11}C production at 0° in reaction of ^{16}O on ^{9}C at 2.1 GeV/nucleon.

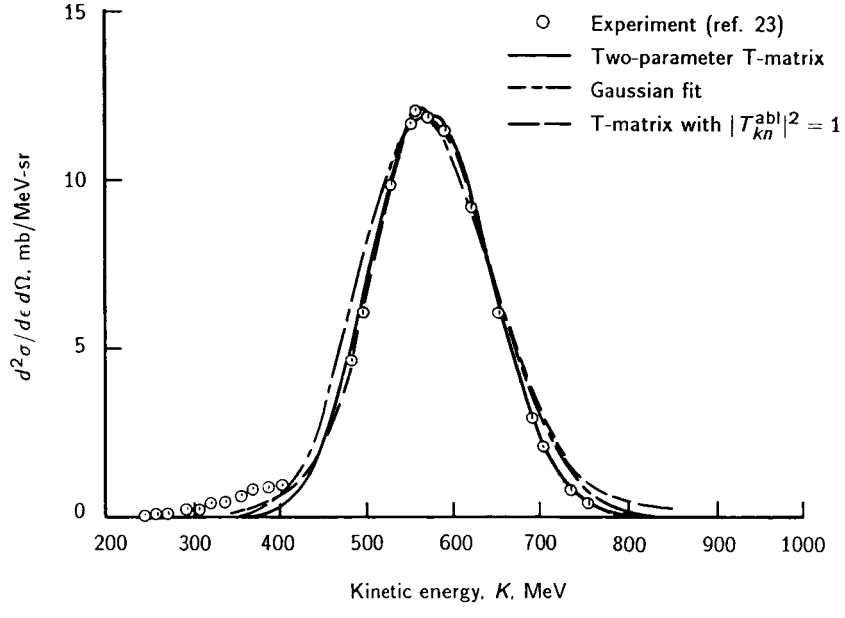

(b) For ^{7}Be production at 4° in reaction of ^{12}C on ^{12}C at 86 MeV/nucleon.

Figure 7. Comparison of fits to doubly differential cross sections.

Standard Bibliographic Page

1. Report No.	2. Government Accession No.	3. Recipient's Catalog No.
NASA TP-2659		

4. Title and Subtitle	5. Report Date
Doubly Differential Cross Sections for Galactic Heavy-Ion Fragmentation	February 1987
	6. Performing Organization Code: 199-22-76-01
7. Author(s): Francis A. Cucinotta, John W. Norbury, Govind S. Khandelwal, and Lawrence W. Townsend	8. Performing Organization Report No.: L-16187
9. Performing Organization Name and Address: NASA Langley Research Center, Hampton, VA 23665-5225	10. Work Unit No.
	11. Contract or Grant No.
12. Sponsoring Agency Name and Address: National Aeronautics and Space Administration, Washington, DC 20546-0001	13. Type of Report and Period Covered: Technical Paper
	14. Sponsoring Agency Code

15. Supplementary Notes

Francis A. Cucinotta, John W. Norbury, and Govind S. Khandelwal: Old Dominion University, Norfolk, Virginia.
Lawrence W. Townsend: Langley Research Center, Hampton, Virginia.

16. Abstract

An abrasion-ablation T-matrix formulation is applied to the calculation of doubly differential cross sections in projectile fragmentation of 2.1 GeV/nucleon ^{16}O on ^{9}Be and 86 MeV/nucleon ^{12}C on ^{12}C and ^{108}Ag. An exponential parameterization of the ablation T-matrix is used and the total width of the intermediate states is taken as a parameter. Fitted values of the total width to experimental results are used to predict the lifetime of the ablation stage and indicate a decay time on the order of 10^{-19} s.

17. Key Words (Suggested by Authors(s))	18. Distribution Statement
Nucleus-nucleus collisions Projectile fragmentation Abrasion-ablation model Doubly differential cross sections	Unclassified—Unlimited Subject Category 73

19. Security Classif.(of this report)	20. Security Classif.(of this page)	21. No. of Pages	22. Price
Unclassified	Unclassified	22	A02

For sale by the National Technical Information Service, Springfield, Virginia 22161

NASA-Langley, 1987